IEEE Access
Multidisciplinary | Rapid Review | Open Access Journal

Received April 1, 2020, accepted April 11, 2020, date of publication April 24, 2020, date of current version May 11, 2020.

Digital Object Identifier 10.1109/ACCESS.2020.2990191

Management and Equalization of Energy Storage Devices for DC Microgrids Using a SoC-Sharing Function

THALES AUGUSTO FAGUNDES[1], GUILHERME HENRIQUE FAVARO FUZATO[2], CASSIUS ROSSI DE AGUIAR[3], KLEBBER DE ARAUJO OTTOBONI[1], MAURICIO BICZKOWSKI[4], AND RICARDO QUADROS MACHADO[1], (Senior Member, IEEE)

[1]School of Engineering, University of São Paulo, São Carlos 13566-590, Brazil
[2]Federal Institute of Education, Science and Technology of São Paulo, Campinas 13059-581, Brazil
[3]Department of Computer Engineering, Federal University of Technology–Paraná, Toledo 85902-490, Brazil
[4]Copel Distribution, Curitiba 81200-240, Brazil

Corresponding author: Thales Augusto Fagundes (thales.fagundes@usp.br)

This work was supported by the Coordination for the Improvement of Higher Education Personnel (CAPES) under grant PDSE-88881.187771/2018-01 and 88881.030370/2013-0, the São Paulo Research Foundation (FAPESP) under grant 2013/20721-4 and the Program for Research and Technological Development of the Electric Energy Sector Regulated by the Brazilian Electricity Regulatory Agency (ANEEL) under grant PD-2866-0454/2016 - Transportable Storage System to Support Scheduled Contingencies at Substations. A partnership between EESC-USP, CPqD and COPEL S.A.

ABSTRACT This paper presents a method for Energy Storage Systems (ESSs) equalization and energy management in dc microgrids (MGs) with slow dynamic sources, such as Fuel Cells (FCs). The three main features of this method are the ESSs equalization, the energy management between the ESSs and the FC, and the ability to suppress fast transients of load, preventing damages in the FC. The equalization is performed using a State of Charge (SoC)-Sharing Function, which is based on a Sigmoid Function (SF). The SoC-Sharing Function is designed similarly to the droop controller, therefore, it is suitable for operation in droop based MGs. Additionally, the ability to suppress fast transients of load is performed by adding a low pass filter in the FC control loop. The main advantages of this method are the SF smooth behavior and the lack of need for a high-speed link of communication between the sources. To evaluate the MG stability, the Lyapunov's Indirect Method is applied in the MG model considering different scenarios varying the SoC and load connected to the dc-link. Finally, the model is validated by comparing simulation and experimental results supplied by a lab-scale prototype.

INDEX TERMS Energy storage system, dc microgrid, equalization method, fuel cell, energy management.

I. INTRODUCTION

The integration of alternative energy sources for grid-tied or standalone operation modes have increased the use of power converters in the worldwide energy matrix. However, the operation of these new devices may produce instabilities due to the alternative energy source nonlinearities, i.e. the wind and solar power are affected by the environmental conditions, while the electrical power produced on the fuel cells (FCs) terminals depends on the chemical reactions between hydrogen (H_2) and oxygen (O_2) [1]–[5].

Additionally, the microgrids (MGs) are the integration of power converters and alternative energy sources with high levels of power quality and stability. In this context, a single alternative energy source connected close to the end-users is named as distributed generation system (DG), while the integration of a considerable number of alternative energy sources is described in the literature as a hybrid power generation system [6]–[8].

The main benefits of a MG is the improvement of power quality, efficiency, stability and economical operation [9]. The replacement of ac to dc DG systems demand financial support as strategy of government and new economical perspectives. However, dc MGs are on continuous rising in comparison with ac MGs because there is no concern to reduce the reactive power and harmonic currents that improves the overall grid performance [3]. For instance, the efficiency of a building energy, that changes from ac to dc technologies rises from 10% to 28% [10].

In addition, dc MGs reduce the conversion losses because the power production is close to the end-users, and it is not required synchronization methods for connect them to a

The associate editor coordinating the review of this manuscript and approving it for publication was Salvatore Favuzza.

common dc-link or to other dc generators [11]. Furthermore, if the dc MG is connected to the main grid, any blackout or voltage sag on the ac-side will not affect the power sources placed on the dc-side [11].

The different rates of wind and solar light may influence the power production on a MG that leads to voltage fluctuation and power unbalances on the dc-side [3]. Thus, Energy Storage Systems (ESSs) are the most suitable solution to mitigate the impacts aforementioned, guaranteeing the reliability, safety and stability [3], [12].

Moreover, there are another benefits that ESSs bring to a dc MG. Among the most important are the compensation of load transients, support for black-start and electrical faults [1], [4], [13], [14]. Although the use of ESSs improve some drawbacks related to the MG operation, they demand a coordination among all sources and ESSs. Otherwise, they may cause deep discharge or over-charge that result in degradation and reduction of their life-cycle [15].

Therefore, a State of Charge (*SoC*) management promotes a balancing among ESS units to prevent different rates of charge/discharge and consequently damages to them [3], [5], [16]. The most effective solution has been widely proposed to improve the dc MG operation to speed up the charge and to reduce the uneven degradation in ESSs [4].

Additionally, the *SoC* equalization can be implemented among their cells or stacks according to the method used on the energy management system [9], [17]. Considering the possibilities, this paper focus on *SoC* battery pack equalization with decentralized strategy, which it does not need a high speed communication link.

In the process of balancing, the units with *SoC* closer to 0% will provide a low amount of power (current), while the units with *SoC* closer to 100% will supply a larger level of power (current) to the dc-link. Moreover at the end of the equaization process, the battery *SoCs* will converge to a similar value.

For the equalization process, one of the main techniques proposed in the literature focus is on the adaptive droop control that changes the virtual resistance according to the *SoC* of each battery in dc MGs. Thus, in [16] a coefficient is responsible to modify the droop slope using the *SoC* and the battery power demand, [18] determines a virtual resistance using the *SoC* as parameter in an exponential function, in [10], the authors propose a coefficient in association with the virtual resistance that depends on the average *SoC* of all storage devices, and [3] applies a fuzzy controller with *SoC* and the voltage error as parameters to calculate the virtual resistance in the strategy of management.

In ac MGs, the equalization presented in [4] proposes an adaptive droop control with a weighting factor obtained from fuzzy inference system with *SoC* as input, while [5] uses a coefficient that depends on the rate that the *SoC* changes.

Moreover, [19] elaborates a different strategy applying *SoC* based droop control that sums a factor to complement the voltage reference from droop management, allowing the balancing process in the dc MG.

TABLE 1. Equalization methods found in literature.

Reference	*Alternative Sources*	*Equalization Method*	*MG Technology*
[3]	PV panels and wind turbine	Adaptive droop control	dc
[4]	PV panels and wind turbine	Adaptive droop control	ac
[5]	PV panels and wind turbine	Adaptive droop control	ac
[10]	Not mentioned	Adaptive droop control	dc
[16]	Not mentioned	*SoC* based droop control	dc
[18]	PV panels and wind turbine	Adaptive droop control	dc
[19]	PV panels	*SoC* based droop control	dc
This paper	Fuel cell	*SoC*-Sharing Function	dc

For stability analysis, [16] and [19] consider only the management control without include the dc-dc converter model while [10] and [18] apply the influence of ESSs connected to their dc-dc converters without evaluate others DG behaviors. In this paper, Lyapunov's Indirect Method contemplates the nonlinear interactions between each dc-dc converter by modeling not only the physical circuit but also the control loops. Additionally, the droop control is not continuously differentiable, thus it is not suitable for proving the level of stability in the whole range of operation.

The comparison of some methods found in literature are shown in Table 1 with the alternative sources presented in the MG, the equalization method and the technology dc or ac.

In this manuscript, the FC is the main source that is integrated on the dc MG by using an interleaved boost with voltage multiplier (IBVM) with high voltage gain, high levels of efficiency and wide capability to process higher input currents [20]. In addition, the dc-link voltage is processed through a droop control to manage the FC terminal current processed by the IBVM.

Each ESS is integrated to the dc MG by a bidirectional buck-boost (BBB) converter, which applies the *SoC*-Sharing Function by using a Sigmoid Function (SF) to manage the power flow from the dc-link to the ESS and to perform the batteries equalization. This function is designed similarly to the droop controller, which is implemented with the dc-link voltage and the *SoC* as input parameters, resulting in a current reference to the BBBs.

Although the SF is nonlinear, it is used to accelerate the approach of batteries' *SoC*. Thus, the SF shape is important in decide whether the batteries should delivery or absorb current according to the dc-link voltage. Moreover, to apply the stability analysis using the Lyapunov's Indirect Method, the system must be modeled using continuously differentiable equations.

According to the FC slow dynamic response, a method to compensate or absorb transients is also applied to reduce damages on FC terminals and increase the MG reliability

[13], [20], [21]. This method of energy management in association with the ESSs, reduces the FC speed response during maneuver of load, and it allows the ESSs to supply power at steady-state to the dc-link.

Finally, Lyapunov's Indirect Method is applied to prove the dc MG stability around the operation region through the dc MG average model, considering the closed loop average model of each dc-dc converter connected to the common capacitor. Therefore, the nonlinear interaction between the modules and control structure are not neglected and the droop control management in the FC is also approximated by a SF to apply the Lyapunov's Indirect Method. The first analysis relates the range of loads that the dc MG was designed to operate. Afterwards, the stability is evaluated by analysing the dc MG eigenvalues for different values of SoC. In addition, an experimental setup is used to demonstrate the effectiveness of the proposed approach.

The following paper is summarized as follows. Section II presents the topology of dc MGs in the standalone mode. Section III presents the function proposed for the dc MG energy management with droop control applied on the FC and the SoC-Sharing Function method to equalize the ESSs. In section IV, the dc MG stability is evaluated using the Lyapunov's Indirect Method. Section V shows the results obtained from the experimental setup in comparison with the computational simulations and numerical solution of MG model using differential equations.

II. MICROGRID CONFIGURATION

Fig. 1 shows the MG selected as case of study, which is composed by a FC, two groups of ESSs and dc loads ($R_1 \ldots R_n$) that represent the local costumers and the equivalent model of the ac-side.

In this context, the main source is a 1 kW proton-exchange membrane (PEM) FC supplied by a tank of H_2 with high levels of purity (around 99.999%). The electronic interfaced connected to the FC terminals is an IBVM with high voltage gain, high efficiency and low ripple level on the current absorbed from the energy source. Furthermore, the architecture of the ESS considered is composed by a BBB converter and battery stacks of two Li-Po in series connection, 5 Ah of capacity and rated voltage of 22.2 V each, resulting in 44.4 V of terminal voltage per stack, as indicated in Fig. 1 [3].

A. SYSTEM DESCRIPTION

In Fig. 2, the ESS terminal voltages and currents are v_{bat1} and i_{in_bat1} for ESS1 and v_{bat2} and i_{in_bat2} for ESS2, respectively. Additionally, the BBBs input low pass filters L_{bat1} C_{bat1} and L_{bat2} C_{bat2} are designed to reduce the ESSs current ripple. In addition, through BBB inductances L_{bat1} and L_{bat2} are flowing i_{Lbat1} and i_{Lbat2}, while v_{Cbat1} and v_{Cbat2} are the voltages on C_{bat1} and C_{bat2}, respectively.

Also in this figure, the FC terminal voltage and current are v_{fc} and i_{in_fc} and the voltages v_{C1} and v_{C2} are measured on the capacitances of the doubler-voltage C_1 and C_2, respectively.

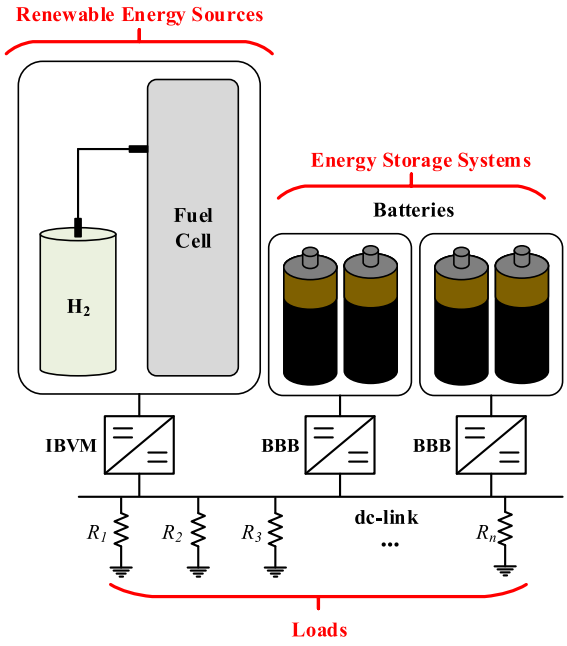

FIGURE 1. MG general structure.

Through the IBVM inductances (L_1 and L_2) are flowing i_{L1} and i_{L2}, thus, the converter input current is defined by $i_{in\_fc} = i_{L1} + i_{L2}$.

In the same picture, the voltage on the common capacitance C_o is v_{link} and i_{link} is the current through the dc load (R_1, R_2, R_3, ...and R_n). Furthermore, $\dot{e}_{fc}$, $\dot{e}_{bat1}$ and $\dot{e}_{bat2}$ are the differences between the current reference and the current measured on the FC, ESS1 and ESS2, respectively, while the terminal capacitance of each dc-dc converter connected in parallel are represented by the equivalent capacitor C_o (considering "n" dc-dc converters, the equivalent capacitor C_o is $C_1 + C_2 + \ldots + C_n$).

B. CONTROL DESCRIPTION

The ESS current references (i_{ref_bat1} and i_{ref_bat2}) are produced according to the dc-link voltage (v_{link}) and the ESS SoC (SoC_1 or SoC_2) values, i.e. v_{link}, SoC_1 or SoC_2 are processed through the SoC-Sharing Function to generate the ESS current references as shown in Fig. 2. Later, the ESS current references (i_{ref_bat1} and i_{ref_bat2}) are compared with the current measured on the ESS terminals (i_{in_bat1} and i_{in_bat2}) and processed through the battery controllers, which, in general, are the classical proportional-integral (PI) controller [13].

Additionally, in Fig. 2, the FC control structure is based on the classical droop control with v_{link} as input and i_{droop_fc} as output. Taking into account the FC characteristics, the power sharing management is used to control the FC dynamic response by adjusting the low pass filter coefficients in the transfer function ($n_d(s)$). Thus, the output current of droop controller (i_{droop_fc}) is processed through the low pass filter to produce the FC current reference (i_{ref_fc}) that is compared

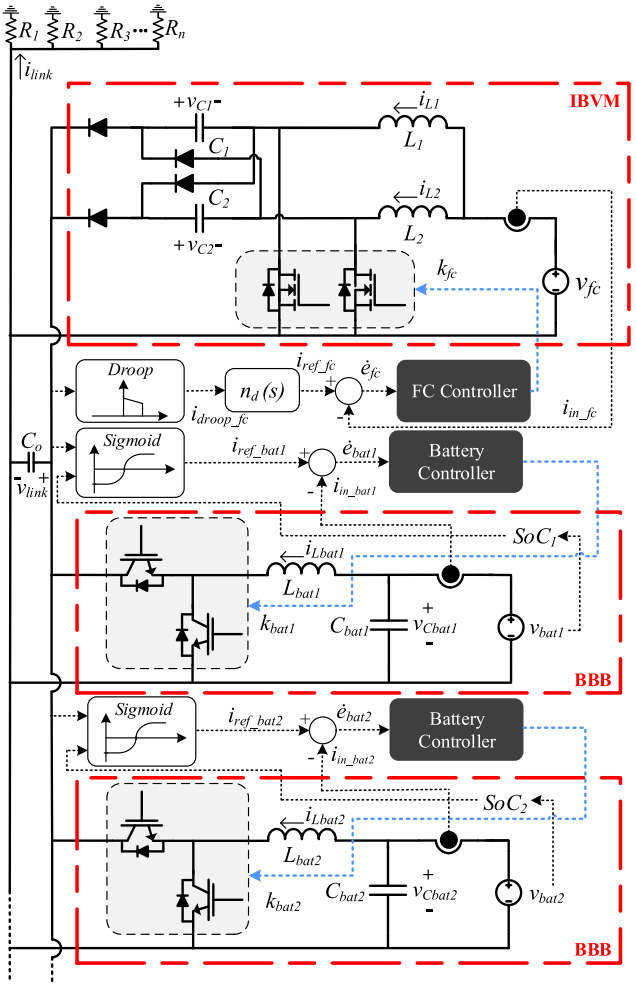

FIGURE 2. MG control diagram.

with the FC measured current (i_{in_fc}) and applied as input in the FC controller (PI compensator).

III. MANAGEMENT AND EQUALIZATION METHODS

The MG controller is responsible to coordinate the current injected or absorbed from the dc-link, where the main challenge is the MG management and equalization considering the ESS fast dynamic and the FC slow dynamic response at transitory regime. To achieve the main requirements of stability, the droop controller is applied on the FC and the *SoC*-Sharing Function defines the current reference of each battery in order to promote the ESS equalization.

A. DROOP CONTROL APPLIED ON THE FUEL CELL MANAGEMENT

The FC energy management function is based on the droop control technique. Therefore, the current reference is defined according to v_{link} [22], [23]. Fig. 3 clarifies the droop control concept, which presents graphically the relationship between the current (i_{droop_fc}) in *p.u.* (per unit) and the dc-link voltage

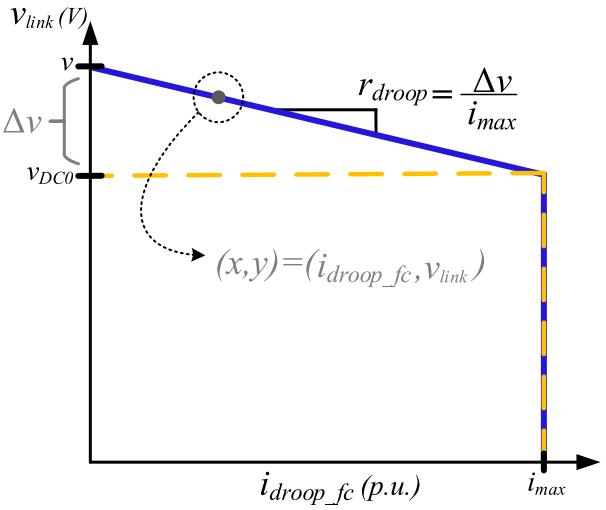

FIGURE 3. Classical droop operation.

(v_{link}). As a result, it is created the concept of the virtual resistance $r_{droop} = \Delta v / i_{max}$ [11].

In this formulation $\Delta v = v - v_{DC0}$, with v being the voltage when $i_{droop\_fc} = 0$ and v_{DC0} the voltage when $i_{droop\_fc} = i_{max}$, with i_{max} representing the maximum current produced by the FC, thus the FC current reference is controlled according to the v_{link} behavior. Additionally, the virtual resistance and the limit of current i_{max} have to be in accordance with the FC limits. Thus, the droop curve from Fig. 3 is defined analytically in (1), where a is the curve slope (the inverse of virtual resistance) in $p.u./V$ and b is the linear coefficient in $p.u.$.

$$i_{droop\_fc} = -\frac{v_{link}}{r_{droop}} + \frac{\Delta v + v_{DC0}}{r_{droop}} = -a\, v_{link} + b \qquad (1)$$

In this context, it is integrated the ESSs and the FC, proposing the ESS dynamic response at transitory regime faster than the FC time response as illustrated in Fig. 4 [24].

To achieve these requirements, the ESS current (i_{in_bat}) has to show a complementary behavior in comparison with the FC current (i_{in_fc}) when a step of load is applied on the dc-link. In other words, the ESS current response has to be faster than the FC current response during load transients.

After that, the FC current achieves the steady-state regime slowly, while the ESS current returns to zero as shown in Fig. 4. The case that the ESS is absorbing the transients and sharing power at steady-state regime will be explained in III-C.

Also in Fig. 4, it is important that the ESS has the capacity to supply enough power to mitigate the load transients, avoiding permanent damage to the FC membrane and ensuring the dc-link stability.

To control the FC speed response (2), the authors include a low pass filter $n_d(s)$ in series with the droop controller to speed up or slow down the FC current response [13].

$$n_d(s) = \frac{1}{(s\tau + 1)} \qquad (2)$$

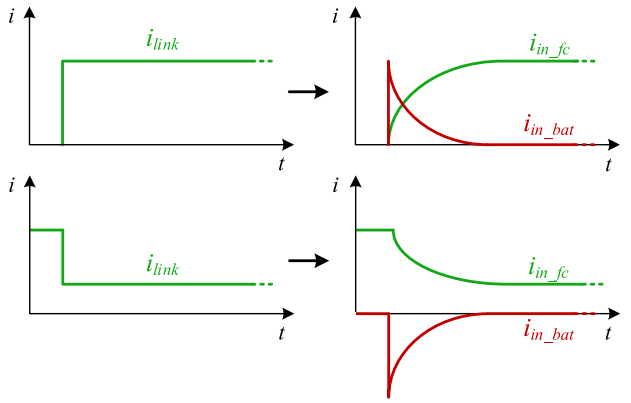

FIGURE 4. MG current behavior during the load transients.

In (2), τ is the time-constant predefined by the designers or adjusted dynamically to match the FC dynamic, which is related to the speed response that the reaction takes to reach an equilibrium.

To evaluate the effectiveness of the FC control scheme, the authors apply the final value theorem (3) on the step response of $i_{droop\_fc}(s)$ in series with the low pass filter $n_d(s)$. The result shows that the low pass filter does not affect the solution at steady-state regime. As consequence, the FC current reference is equal to the FC droop output at steady-state ($I_{ref\_fc} = I_{droop\_fc}$).

$$I_{ref\_fc} = \lim_{s\to 0} I_{droop\_fc} s \frac{1}{s}\frac{1}{s\tau + 1} = I_{droop\_fc} \tag{3}$$

Therefore, it is proved that $n_d(s)$ does not produce alteration in the MG management control structure at steady-state. In addition, as the communication link among the sources is not mandatory, a simple PI is enough to maintain the IBVM at the reference of current according to v_{link}.

For this project, as shown in Fig. 5, it is considered $v_{DC0} = 150\ V$, $\Delta v = 20\ V$, v_{link} in the range of 150-170 V and the maximum current supplied by the FC is 20 A (1 $p.u.$), thus it is followed (4).

$$i_{droop\_fc} = -0.05 v_{link} + 8.5 \tag{4}$$

B. SoC-SHARING FUNCTION FOR THE ESS EQUALIZATION

According to the previous sections, the ESSs operating with *SoCs* numerically equivalents improve the MG efficiency and avoid damage on them. To achieve the aforementioned requirements, the *SoC* of each ESS is estimated with a classical real time algorithm (Coulomb Counting Method), then, they are used as input of the equalization method. In addition, to calculate a new value of i_{ref_bat} properly the equalization method also applies the dc-link voltage (v_{link}) as input, as described in (5).

$$i_{ref\_bat} = \frac{2}{1 + e^{(e_{factor} - SoC)10}} - 1 \tag{5}$$

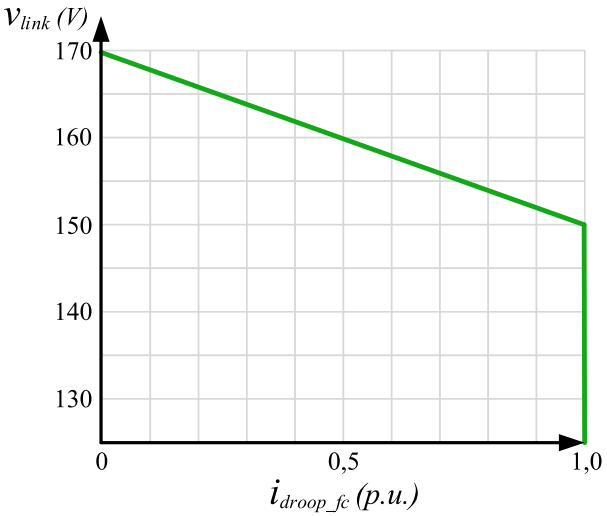

FIGURE 5. Relationship between i_{droop_fc} and v_{link}.

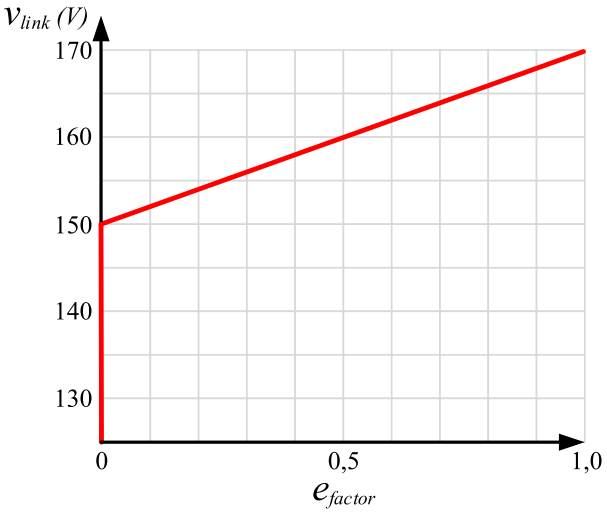

FIGURE 6. Behavior of the equalization factor.

where e_{factor} is the equalization factor defined according to (6).

$$e_{factor} = \frac{v_{link} - v_{DC0}}{\Delta v} \tag{6}$$

In accordance with voltage range of droop control, it is defined the range of e_{factor} as 150-170 V, as shown in Fig. 6. From this analysis, if e_{factor} is closed to zero, there is a smoothly equalization process to avoid the MG instability because the dc-link approaches to the maximum capacity of operation (minimum dc-link voltage). However, the ESS balancing is easily achieved when v_{link} is close to 170 V, because the load demand on the dc-link is slight.

Fig. 7 shows the surface formed by plotting (5), where the ESS current reference (i_{ref_bat}) is defined from -1 $p.u.$ to 1 $p.u.$, considering negatives values for charging and positives for discharging, while *SoC* varies from 0% to 100% and v_{link} is in the range of 150-170 V.

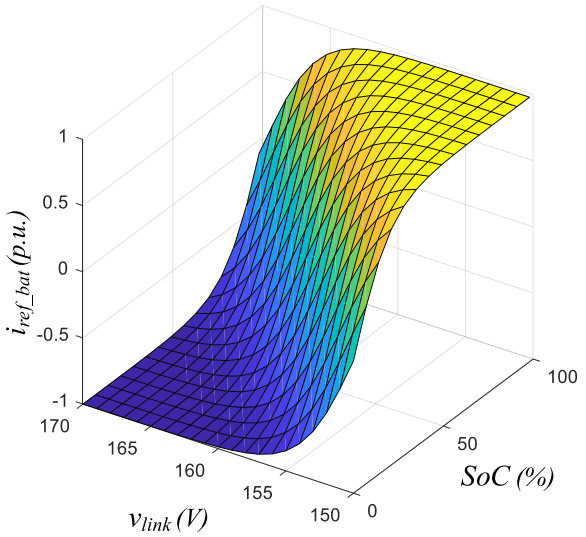

FIGURE 7. ***SoC*-Sharing Function waveform.**

In order to improve the analysis, Fig. 8 shows the *SoC*-Sharing Function in 2-D (two dimensions) according to 3 different dc-link voltages, with the maximum capacity of load ($v_{link} = 150\ V$), with half capacity ($v_{link} = 160\ V$) and without load connected to the MG ($v_{link} = 170\ V$). In these scenarios, the ESSs can supply power (delivery current) when the maximum load is connected to the MG or absorb power (absorb current) when the dc-link has not load connected to its terminals.

Finally, Fig. 9 shows the *SoC*-Sharing Function surface in 2-D according to 3 cases of *SoC*: 0%, 50% and 100%. Note that there is an unique possibility of charging in the whole range of the dc-link with ESS completely discharged, while the ESS can only supply current when its *SoC* is around 100%, avoiding over charging.

According to Fig. 8 and Fig. 9, the ESS with *SoC* numerically high can absorb or deliver current in accordance with the dc-link load. For this case, if v_{link} is around 170 V, the battery is charged because the load demand on the dc-link is slight; otherwise, if v_{link} is around 150 V, a heavy load is connected to the dc-side and the ESS must increase the discharging current to avoid the dc-link collapse.

In the opposite case, when the ESS is completely discharged, indicating a *SoC* numerically low, it can be charged by the extra power available on the dc-link. To become a simple evaluation of the proposed method, Table 2 presents the logic applied for the management of the dc MG using the *SoC*-Sharing Function for ESS equalization.

Therefore, the *SoC*-Sharing Function guarantees that the storage devices balance their *SoCs* in the MG, and then the ESSs are operated with a similar charging current. Because of the *SoC* is a parameter that establishes a long time to change (depends on battery capacity) [5], [25], the *SoC*-Sharing Function is also responsible for the dc-link current management, as illustrated in Fig. 10 that

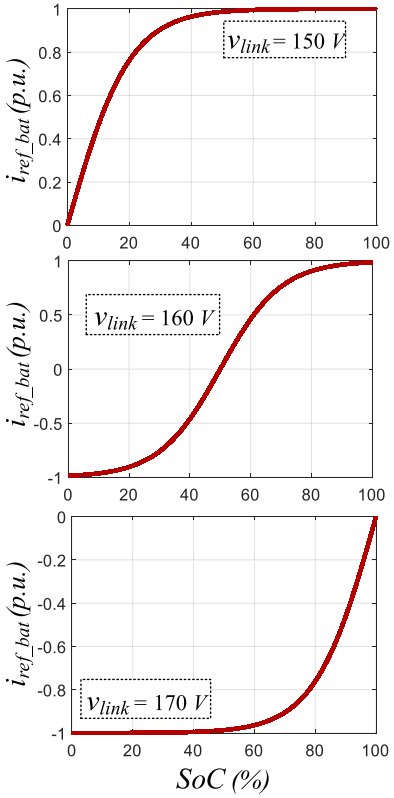

FIGURE 8. **Relationship between i_{ref_bat} and *SoC* considering v_{link} constant for 3 different cases.**

TABLE 2. **Battery action according to *SoC* and v_{link}.**

SoC	v_{link}	*Battery Current Range*
high (above 80%)	high (around 170 V)	-0.4 to 0.0 $p.u.$
middle (around 50%)	high	-1.0 to -0.8 $p.u.$
low (below 30%)	high	-1.0 $p.u.$
high	middle (around 160 V)	0.9 to 1.0 $p.u.$
middle	middle	0.0 $p.u.$
low	middle	-1.0 to -0.9 $p.u.$
high	low (around 150 V)	1.0 $p.u.$
middle	low	0.9 to 1.0 $p.u.$
low	low	0.0 to 0.4 $p.u.$

presents i_{ref_bat} *vs.* v_{link} according with level of *SoC* (from 0% until 100%).

C. SoC-SHARING FUNCTION FOR THE TRANSITORY AND STEADY-STATE REGIMES

As mentioned in subsection II-B, the FC current is associated with a low pass first order filter that leads to a slower response when the loads are changed on the dc-side. To improve the MG stability, the ESSs are used to compensate/absorb transients on the dc-link. This feature is associated with the v_{link} measurement in the *SoC*-Sharing Function, then, any load variation on dc-link implies on changes in i_{in_bat}. As a result, the *SoC*-Sharing Function maintains the equalization and leads the ESS to a fast response at transitory

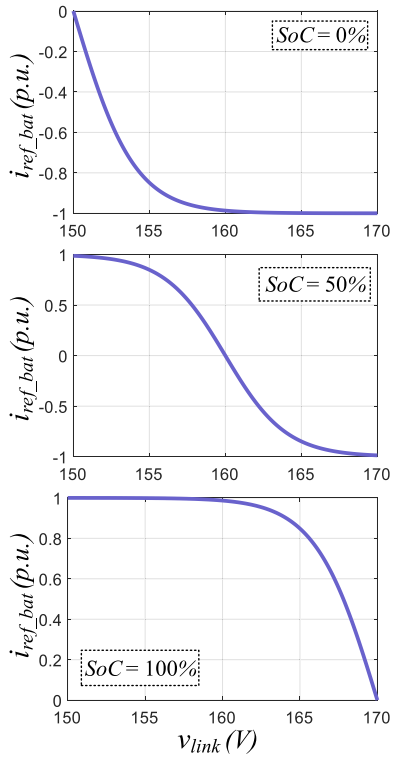

FIGURE 9. Relationship between i_{ref_bat} and v_{link} considering *SoC* constant for 3 different cases.

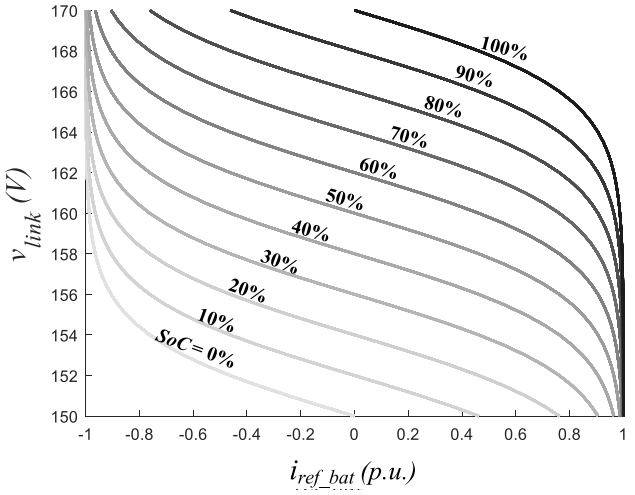

FIGURE 10. Effects of the *SoC* on the ESS contribution.

while it shares, at steady-state regime, the amount of power injected in the dc-link in contribution with the FC, as shown in Fig. 11.

IV. DC MICROGRID STABILITY

Due to an enormous variety of DGs with different dynamics behavior, a stability analysis is important to ensure that any load variations does not lead the MG to an unstable operation on the dc-side [26]. In this work, it is considered the complete interactions between the dc-units, i.e. the dc-dc converter's

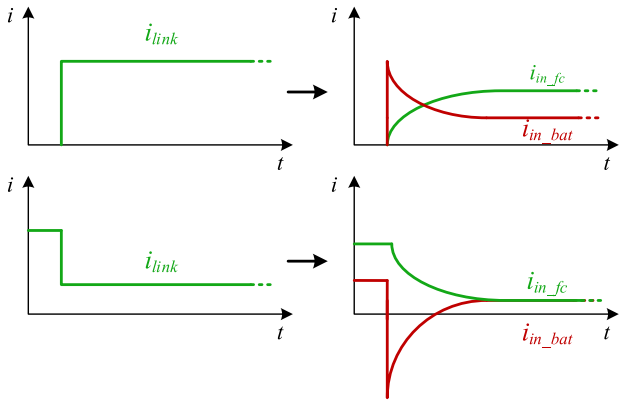

FIGURE 11. MG current behavior during the transients and steady-state.

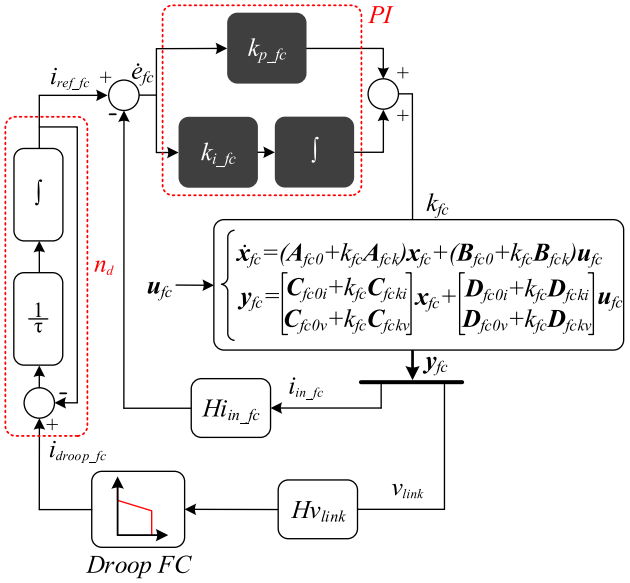

FIGURE 12. FC control scheme.

close loop average model (CLAM) coupled with the dc-link capacitor (C_o) via differential equation is calculated. Later, the eigenvalue analysis on the CLAM via Lyapunov's Indirect Method is performed considering two cases: variations on the dc loads with constant *SoC* of all ESSs and the changes on *SoC* according to their balancing with constant dc load. Thus, the subsections IV-A and IV-B evaluate a detailed control loop of the FC and the ESS, respectively, and then, the subsection IV-C considers the coupled model of all DGs units on MG.

A. FC CONTROL LOOP

Fig. 12 shows the FC control loop considering that in the inner loop the IBVM current (i_{in_fc}) is controlled by a proportional-integrator (PI) controller with k_{p_fc} and k_{i_fc} as the controller gains. Also in Fig. 12, the outer loop applies the droop technique integrated with the low pass filter ($n_d(s)$)

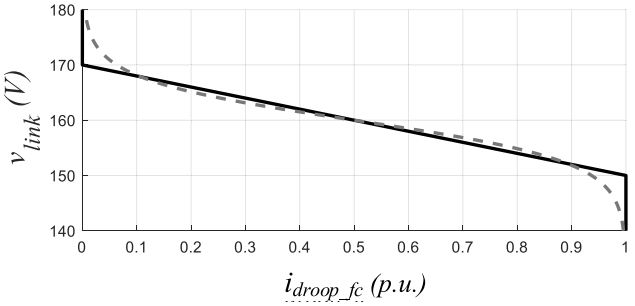

FIGURE 13. FC virtual resistance using a linear equation in solid line and SF approximation in dashed line.

to adjust the FC speed response according to the time constant (τ).

In the same picture, Hi_{in_fc} and Hv_{link} are the gains of the current and voltage sensors. Regarding the IBVM model, $\boldsymbol{A}_{fc0}$, $\boldsymbol{B}_{fc0}$, $\boldsymbol{C}_{fc0i}$, $\boldsymbol{C}_{fc0v}$, $\boldsymbol{D}_{fc0i}$ and $\boldsymbol{D}_{fc0v}$ are the state, input, output and feed-forward matrices at steady-state. Moreover, $\boldsymbol{A}_{fck}$, $\boldsymbol{B}_{fck}$, $\boldsymbol{C}_{fcki}$, $\boldsymbol{C}_{fckv}$, $\boldsymbol{D}_{fcki}$ and $\boldsymbol{D}_{fckv}$ are the state, input, output and feed-forward matrices around the operation point, as calculated according to [27].

Also in Fig. 12, $\dot{\boldsymbol{x}}_{fc}$, $\boldsymbol{y}_{fc}$, $\boldsymbol{u}_{fc}$ and k_{fc} are the FC vector of states, output, input and the FC duty-cycle, respectively. Furthermore, the output vector is defined as $\boldsymbol{y}_{fc} = [i_{in\_fc}\ v_{link}]^T$, the state vector as $\boldsymbol{x}_{fc} = \begin{bmatrix} i_{L1}\ i_{L2}\ v_{C1}\ v_{C2}\ v_{link} \end{bmatrix}^T$ and the input vector as $\boldsymbol{u}_{fc} = \begin{bmatrix} v_{fc}\ i_{link} \end{bmatrix}^T$.

As the Lyapunov's Indirect Method is applied to systems that are continuously differentiable, the droop virtual resistance, illustrated in Fig. 13, is approximated by another SF (7), with α_{fc} representing the curve slope and β_{fc} the curve translation. For this case, $\alpha_{fc} = 0.2696$ and $\beta_{fc} = 160$.

$$i_{droop\_fc} = 1 - \frac{1}{1 + \mathrm{e}^{-\alpha_{fc}(v_{link}Hv_{link} - \beta_{fc})}} \tag{7}$$

In Fig. 13, the solid line represents the droop curve using a linear equation while the SF is represented by the dashed line. In both curves, if the dc-link voltage is higher than 170 V, the droop setpoint i_{droop_fc} is null. Between 170 V and 150 V, the droop setpoint is associated with the linear equation. Finally, if the dc-link voltage is below 150 V, the setpoint reaches the maximum value at 1 $p.u.$.

B. ESS CONTROL LOOP

Fig. 14 presents the ESS control loop considering that in the inner loop the BBB input current (i_{in_bat}), measured with a sensor of gain Hi_{in_bat}, is controlled by a PI controller with k_{p_bat} and k_{i_bat} representing their gains. The outer loop is responsible for the energy management algorithm, which employs the *SoC*-Sharing Function using the dc-link voltage, measured with a sensor of gain Hv_{link}, and *SoC* as inputs. The output of the *SoC*-Sharing Function generates the inner loop reference with the variable i_{ref_bat}.

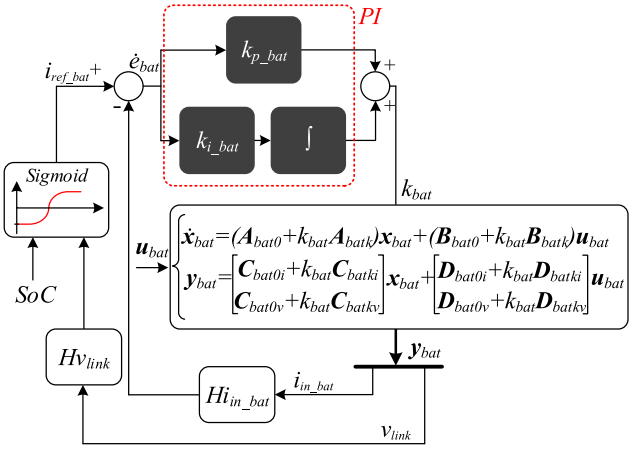

FIGURE 14. ESS control scheme.

Regarding the BBB model, $\boldsymbol{A}_{bat0}$, $\boldsymbol{B}_{bat0}$, $\boldsymbol{C}_{bat0i}$, $\boldsymbol{C}_{bat0v}$, $\boldsymbol{D}_{bat0i}$ and $\boldsymbol{D}_{bat0v}$ are the state, input, output and feed-forward matrices at steady-state regime. Furthermore, $\boldsymbol{A}_{batk}$, $\boldsymbol{B}_{batk}$, $\boldsymbol{C}_{batki}$, $\boldsymbol{C}_{batkv}$, $\boldsymbol{D}_{batki}$ and $\boldsymbol{D}_{batkv}$ are the state, input, output and feed-forward matrices around the operation point, as calculated according to [27].

Also in Fig. 14, $\dot{\boldsymbol{x}}_{bat}$, $\boldsymbol{y}_{bat}$, $\boldsymbol{u}_{bat}$ and k_{bat} are the ESS vector of states, output, input and the ESS duty-cycle, respectively. Additionally, it is considered that the output vector is defined by $\boldsymbol{y}_{bat} = [i_{in\_bat}\ v_{link}]^T$, the state vector is $\boldsymbol{x}_{bat} = \begin{bmatrix} v_{Cbat}\ i_{Lbat}\ v_{link} \end{bmatrix}^T$ and the input vector is $\boldsymbol{u}_{bat} = \begin{bmatrix} v_{bat}\ i_{link} \end{bmatrix}^T$.

C. DC MICROGRID AVERAGE MODEL

Finally, the dc MG average model (8) is obtained by considering the closed loop average model of each dc-dc converter described in the subsections IV-A and IV-B.

In (8), the first differential equation, $\dot{v}_{link}$, is related to the dc-link voltage. As there are three dc DG systems integrated on the MG, the load contribution has to be decremented twice $\left(2(-\frac{v_{link}}{R_o C_o})\right)$ to avoid superposition. The next three differential equations consists of $\dot{\boldsymbol{x}}_{fc}^{(1:4)}$, $\dot{\boldsymbol{e}}_{fc}$ and $\dot{\boldsymbol{i}}_{ref\_fc}$. In addition, the fifth and the sixth equation ($\dot{\boldsymbol{x}}_{bat1}^{(1:2)}$ and $\dot{e}_{bat1}$) are related to the ESS1 with $\boldsymbol{x}_{bat1} = \begin{bmatrix} v_{Cbat1}\ i_{Lbat1}\ v_{link} \end{bmatrix}^T$. The seventh and the last equation ($\dot{\boldsymbol{x}}_{bat2}^{(1:2)}$ and $\dot{e}_{bat2}$) are associated to the ESS2 with $\boldsymbol{x}_{bat2} = \begin{bmatrix} v_{Cbat2}\ i_{Lbat2}\ v_{link} \end{bmatrix}^T$. Finally, the ESS1 input vector is $\boldsymbol{u}_{bat1} = \begin{bmatrix} v_{bat1}\ i_{link} \end{bmatrix}^T$ and ESS2 input vector is $\boldsymbol{u}_{bat2} = \begin{bmatrix} v_{bat2}\ i_{link} \end{bmatrix}^T$.

It is important to notice that in the matrix indices for the FC and ESS state vectors are (1:4) and (1:2), respectively. These indices are used to avoid repetition of the dc-link voltage differential equation.

V. STABILITY ANALYSIS

In the stability analysis, the real part of the eigenvalues are calculated using the Jacobian's matrix of (8). Additionally,

to avoid damages on the FC and ESSs, it is considered that the maximum FC current (I_{fc_max}) is 20 A and the maximum ESS current (I_{bat_max}) is 5 A.

Firstly, it is addressed the effect of the load variations in the dc-link considering the other parameters as constants. Afterwards, it is analyzed the stability during the equalization process. Considering that the dynamic response associated with the rate of SoC is much slower when compared with the current and voltages variables in (8), as shown at the bottom of this page, the stability analysis is performed and presented for constant values of SoC.

For this purpose, the MG is analyzed in two different cases. In the first case, the ESS1 is practically discharged with $SoC_1 = 10\%$, while ESS2 is charged at medium range with $SoC_2 = 40\%$. In the second case, the ESS1 presents $SoC_1 = 20\%$, while ESS2 is almost fully charged with $SoC_2 = 80\%$.

A. EFFECT OF THE LOAD POWER VARIATION ON THE DC MG STABILITY

For this analysis, Fig. 15 shows the eigenvalues of the Jacobian matrix for a specified range of load connected to the dc-link. For $SoC_1 = 10\%$ and $SoC_2 = 40\%$, without load connected implies in $v_{link} = 159\ V$ while the maximum value of load (680 W) leads to $v_{link} = 152\ V$. However, for $SoC_1 = 20\%$ and $SoC_2 = 80\%$, without load connected implies in $v_{link} = 164\ V$ while the maximum value of load (680 W) leads to $v_{link} = 153\ V$. As the first case have the ESSs with SoC_1 and SoC_2 lower than the second case, the power consumed by the batteries is higher for the first case. Thus, the dc-link voltage sweeps in a higher range for the second case.

Therefore, the load incremented moves the eigenvalues straightforward to the right side of the imaginary frame. Fortunately, this action is not sufficient to shift the eigenvalues of the dc MG to the region of instability. With the load increment in the specified range, the dc-link voltage sweeps range of operation on the droop line according with the SoC of both ESS.

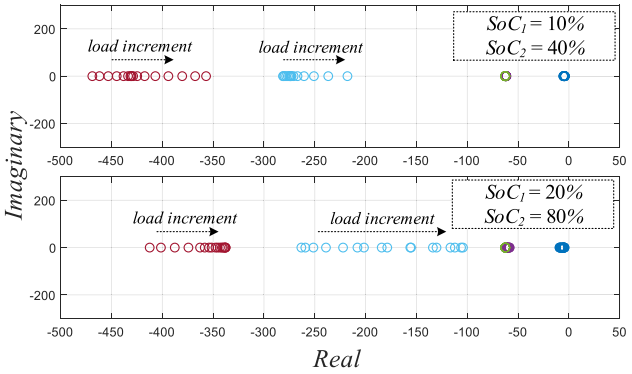

FIGURE 15. Movement of the eigenvalues in the complex plane for different values of load for the coupled MG.

B. STABILITY ANALYSIS DURING THE EQUALIZATION PROCESS

To perform the stability analysis during the equalization process, the authors propose the SoC changing for each operation point. In this context, the difference of SoC_2 and SoC_1 (ΔSoC) is decreased as the equalization process is reached.

In Fig. 16, the storage balancing process is not able to move the eigenvalues to the right side of the imaginary frame. Moreover, Fig. 17 shows the maximum real part of the eigenvalues ($max(\Re[\lambda_i])$). Although there is a slightly rising of $max(\Re[\lambda_i])$ as the equalization process occurs, this change is not sufficient to shift the dc MG to the instability.

VI. RESULTS

The authors used an experimental test bed to verify the theoretical analysis proposed in this manuscript, as shown in Fig. 18. In this study, the main source is the H-1000 FC from Horizon Technologies with a rated power of 1 kW, while each ESS is represented by a group of two Li-Po batteries in series connection with rated voltage of 22.2 V each, resulting in a total of 44.4 V. Moreover, the maximum current supplied by the FC is 20 A, while the battery pack supplies/absorbs

$$
\begin{bmatrix} \dot{v}_{link} \\ \dot{\boldsymbol{x}}_{fc}^{(1:4)} \\ \dot{e}_{fc} \\ i_{ref\_fc} \\ \dot{\boldsymbol{x}}_{bat1}^{(1:2)} \\ \dot{e}_{bat1} \\ \dot{\boldsymbol{x}}_{bat2}^{(1:2)} \\ \dot{e}_{bat2} \end{bmatrix} = \begin{bmatrix} \begin{bmatrix} \boldsymbol{x}_{fc} \\ \boldsymbol{x}_{bat1} \\ \boldsymbol{x}_{bat2} \end{bmatrix}^T \begin{bmatrix} \boldsymbol{A}_{fc0}^{(5,1:5)} + k_{fc}\boldsymbol{A}_{fck}^{(5,1:5)} \\ \boldsymbol{A}_{bat10}^{(3,1:3)} + k_{bat1}\boldsymbol{A}_{bat1k}^{(3,1:3)} \\ \boldsymbol{A}_{bat20}^{(3,1:3)} + k_{bat2}\boldsymbol{A}_{bat2k}^{(3,1:3)} \end{bmatrix} + \cdots \\ \cdots + \begin{bmatrix} \boldsymbol{u}_{fc} \\ \boldsymbol{u}_{bat1} \\ \boldsymbol{u}_{bat2} \end{bmatrix}^T \begin{bmatrix} \boldsymbol{B}_{fc0}^{(5,1:2)} + k_{fc}\boldsymbol{B}_{fck}^{(5,1:2)} \\ \boldsymbol{B}_{bat10}^{(3,1:2)} + k_{bat1}\boldsymbol{B}_{bat1k}^{(3,1:2)} \\ \boldsymbol{B}_{bat20}^{(3,1:2)} + k_{bat2}\boldsymbol{B}_{bat2k}^{(3,1:2)} \end{bmatrix} - 2(-\frac{v_{link}}{R_o C_o}) \\ (\boldsymbol{A}_{fc0}^{(1:4,1:5)} + k_{fc}\boldsymbol{A}_{fck}^{(1:4,1:5)})\boldsymbol{x}_{fc} + (\boldsymbol{B}_{fc0}^{(1:4,1:5)} + k_{fc}\boldsymbol{B}_{fck}^{(1:4,1:5)})\boldsymbol{u}_{fc} \\ i_{ref\_fc} - Hi_{in\_fc} i_{in\_fc} \\ \frac{1}{\tau}[I_{fcmax} i_{droop\_fc} - i_{ref\_fc}] \\ (\boldsymbol{A}_{bat10}^{(1:2,1:3)} + k_{bat1}\boldsymbol{A}_{bat1k}^{(1:2,1:3)})\boldsymbol{x}_{bat1} + (\boldsymbol{B}_{bat10}^{(1:2,1:3)} + k_{bat1}\boldsymbol{B}_{bat1k}^{(1:2,1:3)})\boldsymbol{u}_{bat1} \\ i_{ref\_bat1} - Hi_{in\_bat1} i_{in\_bat1} \\ (\boldsymbol{A}_{bat20}^{(1:2,1:3)} + k_{bat2}\boldsymbol{A}_{bat2k}^{(1:2,1:3)})\boldsymbol{x}_{bat2} + (\boldsymbol{B}_{bat20}^{(1:2,1:3)} + k_{bat2}\boldsymbol{B}_{bat2k}^{(1:2,1:3)})\boldsymbol{u}_{bat2} \\ i_{ref\_bat2} - Hi_{in\_bat2} i_{in\_bat2} \end{bmatrix} \tag{8}
$$

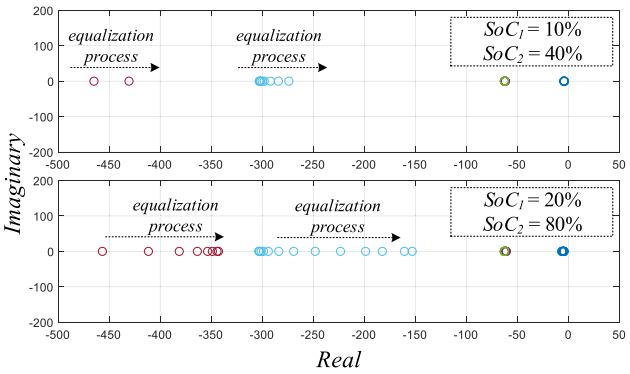

FIGURE 16. Movement of the eigenvalues in the complex plane for the equalization process. First case for $SoC_1 = 10\%$ and $SoC_2 = 40\%$. Second case for $SoC_1 = 20\%$, $SoC_2 = 80\%$. In the both cases, there are 400 W connected to the dc-link that leads to $v_{link} = 158\ V$.

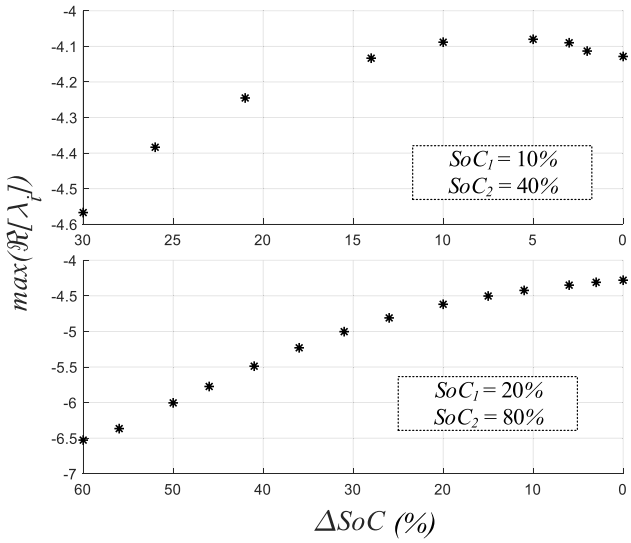

FIGURE 17. Behavior of the maximum real part of the eigenvalues for the equalization process. First case for $SoC_1 = 10\%$ and $SoC_2 = 40\%$. Second case for $SoC_1 = 20\%$, $SoC_2 = 80\%$. In the both cases, there are 400 W connected to the dc-link that leads to $v_{link} = 158\ V$.

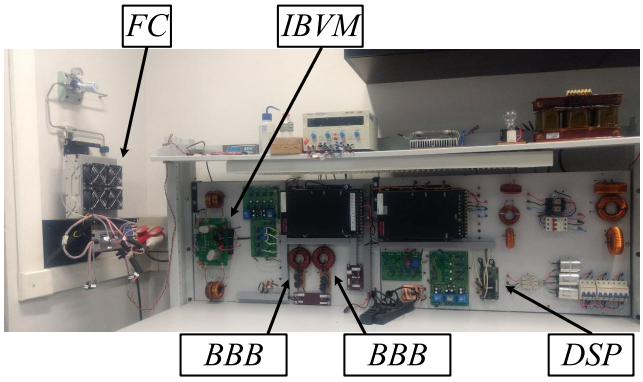

FIGURE 18. Experimental test bed.

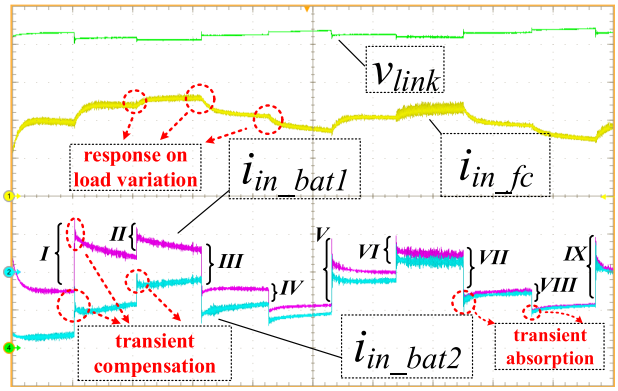

FIGURE 19. MG under load maneuver considering initial $SoC_1 = 10\%$ and $SoC_2 = 40\%$. Vertical: dc-link voltage v_{link} (20 V/div.), FC current i_{in_fc} (5 A/div.), ESS1 current i_{in_bat1} (2.5 A/div.), ESS2 current i_{in_bat2} (2.5 A/div.). Horizontal: time (2 s/div.).

TABLE 3. Switched load values.

Instant	I	II	III	IV	V
Load (Ω)	$\uparrow$ 96.1	$\uparrow$ 190.4	$\downarrow$ 96.1	$\downarrow$ 190.4	$\uparrow$ 96.1
Instant	VI	VII	VIII	IX	*****
Load (Ω)	$\uparrow$ 190.4	$\downarrow$ 96.1	$\downarrow$ 190.4	$\uparrow$ 96.1	*****

a maximum of 5 A. The control scheme was embedded in a 32-bit dual core TMS320F28379D processor from Texas Instruments with a total processing capacity of 800 MIPS.

To evaluate the effectiveness of the proposed approach, this manuscript performs two types of analysis. In the first, the authors relate the equalization process obtained in the test bed with the simulation in the PSIM software. In the second, the experimental results are compared with the differential equations results (8) using the Matlab solver ODE23tb.

A. COMPARISON BETWEEN THE EXPERIMENTAL AND SIMULATION TESTS PERFORMED IN THE PSIM

To speed up the time of analysis and avoid long periods of test, the experiments were scaled with 1 s corresponding to 200 s. Therefore, the real battery pack capacity in 10 Ah, $C_{bat}(real)$, follows the simple model shown in (9), where $C_{bat}(exp)$ is the experimental capacity of the ESS.

$$C_{bat}(real) = 200 C_{bat}(exp) \tag{9}$$

Fig. 19 shows the first experimental results considering initial $SoC_1 = 10\%$ and $SoC_2 = 40\%$. In this test, the behavior of v_{link}, i_{in_fc}, i_{in_bat1} and i_{in_bat2} are indicated. The amount of switching load are present in Table 3, where $\uparrow$ represents an increase and $\downarrow$ a decrease.

As ESS1 is almost fully discharged, it receives a higher amount of current (i_{in_bat1}) than ESS2 (i_{in_bat2}). Thus, the equalization process is accomplished as shown in Fig. 20. It is important to notice that SoC estimation is based on the Coulomb Counting Method.

Batteries are charged only with a high voltage on dc-link while there is a slight load connected to the dc MG. Also in Fig. 20, the dashed line represents simulation results from

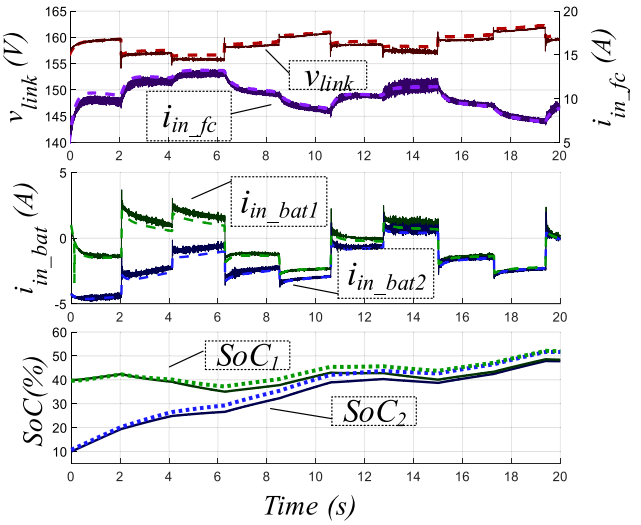

FIGURE 20. MG under load connection considering initial $SoC_1 = 10\%$ and $SoC_2 = 40\%$. The experimental results are showed in the continuous line and the simulations performed in the PSIM are indicated in dashed line.

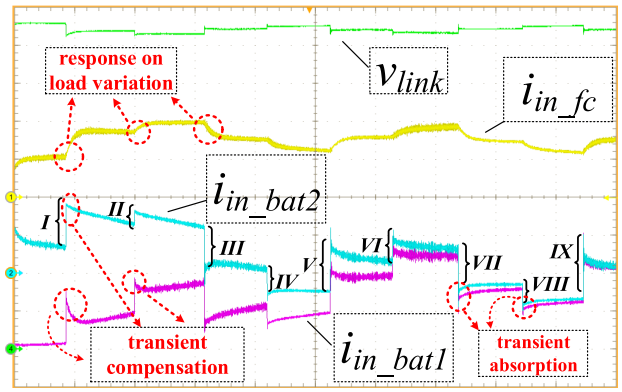

FIGURE 21. MG under load variation considering initial $SoC_1 = 20\%$ and $SoC_2 = 80\%$. Vertical: dc-link voltage v_{link} (20 V/div.), FC current i_{in_fc} (5 A/div.), ESS1 current i_{in_bat1} (2.5 A/div.), ESS2 current i_{in_bat2} (2.5 A/div.). Horizontal: time (2 s/div.).

PSIM, while continuous line is obtained from experimental setup.

The second case considers initial values of $SoC_1 = 20\%$ and $SoC_2 = 80\%$. The behavior of v_{link}, i_{in_fc}, i_{in_bat1} and i_{in_bat2} are followed in Fig. 21 with the load variation on the dc MG operation also according to Table 3. As shown, the equalization performance is related to v_{link}, if there is a significant demand of load on the dc-link, the current reference of the batteries is lower, also according to their *SoCs*. Otherwise, if there is a considerable amount of current absorbed, then, the demand of load on the dc side has to be light. In Fig. 22, *SoC* estimation is also from Coulomb Counting Method and there is a comparison between experimental and simulation results.

For both results of experimental tests in Fig. 19 and Fig. 21, the highest value of FC current is below to the maximum limit

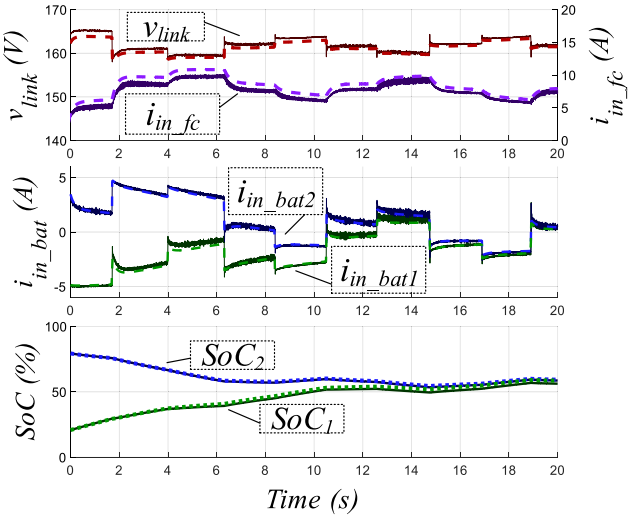

FIGURE 22. MG under load variation operating initial $SoC_1 = 20\%$ and $SoC_2 = 80\%$. Experimental results are in continuous line and simulations from PSIM are in dashed line.

TABLE 4. Switched load values for experimental test of Fig. 23.

Instant	I	II	III	IV
Load (Ω)	$\uparrow$ 96.1	$\uparrow$ 324.4	$\downarrow$ 96.1	$\downarrow$ 324.4

of 20 *A*. Thus, in addition to protect the main source at transitory response, the management and equalization process also avoid damages on FC at steady-state regime.

B. COMPARISON BETWEEN THE EXPERIMENTAL TEST AND THE SOLUTION VIA DIFFERENTIAL EQUATIONS

This subsection presents the comparison between the MG analytical model (8) solutions using the ODE23tb Matlab solver and the experimental results. As the *SoC* changes in a slow rate, for the MG differential equations using ODE23tb, the *SoC* was considered as a constant while for the experimental results were addressed the real battery pack capacity, avoiding the relation (9) as the previous results.

Thus, the experimental results are presented in Fig. 23, which shows the v_{link}, i_{in_fc}, i_{in_bat1} and i_{in_bat2} with load variation according to Table 4. The comparison between the experimental results and the numerical solutions are presented in Fig. 24. In this figure, the numerical solutions were performed considering the *SoC* of the two batteries constant at $SoC_1 = 10\%$ and $SoC_2 = 40\%$.

As shown in Fig. 24, there are some discrepancies in mathematical solution compared to experimental results because the model uses a SF as a reference of FC current control loop, instead of a droop curve. Apart from this, the ESS and FC voltages are considered as constant in mathematical calculation. According to Fig. 23 and Fig. 24, it is noted that ESS1 (i_{in_bat1}) delivers more current than ESS2 (i_{in_bat2}) because they have divergent values of *SoC* that implies on a distinct curves of management, as described in Fig. 10 on subsection III-B.

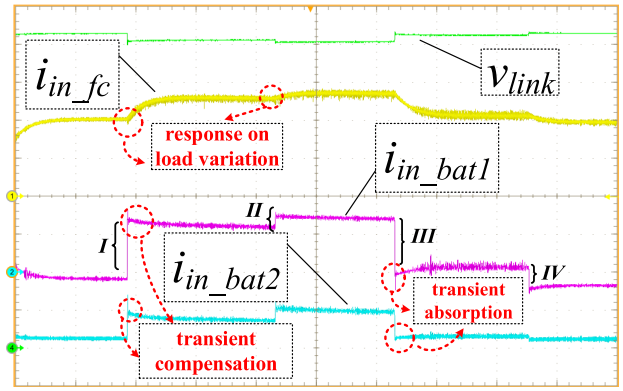

FIGURE 23. MG under load maneuver considering $SoC_1 = 10\%$, $SoC_2 = 40\%$ and the real battery pack capacity. Vertical: dc-link voltage v_{link} (20 V/div.), FC current i_{in_fc} (5 A/div.), ESS1 current i_{in_bat1} (2.5 A/div.), ESS2 current i_{in_bat2} (2.5 A/div.). Horizontal: time (1 s/div.).

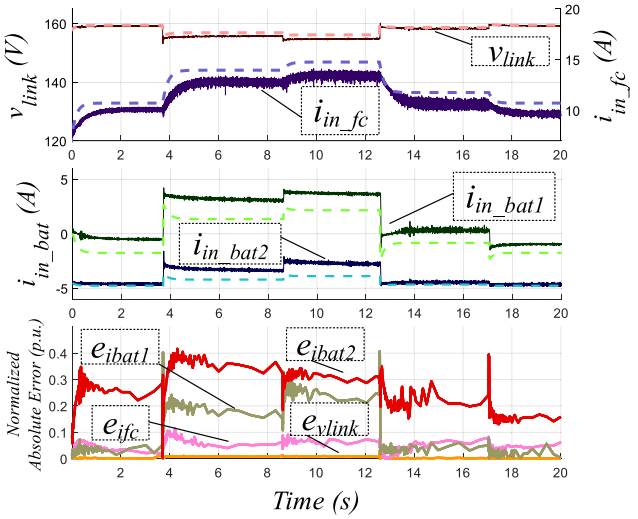

FIGURE 24. MG under load connection considering $SoC_1 = 10\%$ and $SoC_2 = 40\%$. Experimental results are in continuous line and mathematical solution from ODE23tb are in dashed line. The normalized error ($p.u.$) of v_{link}, i_{in_fc}, i_{in_bat1} and i_{in_bat2} are represented by e_{vlink}, e_{ifc}, e_{ibat1} and e_{ibat2}, respectively.

Also in Fig. 24, there are the normalized error ($p.u.$) calculated according to (10), where v_{link}, i_{in_fc}, i_{in_bat1} and i_{in_bat2} are represented by e_{vlink}, e_{ifc}, e_{ibat1} and e_{ibat2}, respectively.

$$e_{normalized} = \frac{|exp_{data} - analytical_{data}|}{rated_{value}} \tag{10}$$

In (10), $e_{normalized}$ is defined in $p.u.$, exp_{data} is the experimental data, $analytical_{data}$ is the result from the analytical model calculated with ODE23tb and $rated_{value}$ is the rated value of each source (160 V for v_{link}, 20 A for i_{in_fc} and 5 A for i_{in_bat1} and i_{in_bat2}). Finally, the Table 5 shows the mean normalized error of results from Fig. 24. As mentioned before, the difference of i_{in_fc}, i_{in_bat1} and i_{in_bat2} is related to the approximation adopted in the mathematical model. Another reason is the difficult to model the nonlinear characteristic of FC related to the membrane humidity, temperature influence and others factors [28].

TABLE 5. Mean normalized absolute error between experimental and analytical test.

Mean Normalized Absolute Error ($p.u.$)	
v_{link}	0.0071
i_{in_fc}	0.0990
i_{in_bat1}	0.1841
i_{in_bat2}	0.3217

VII. CONCLUSION

This paper presented a ESS management using the *SoC*-Sharing Function. The proposed strategy fits to MGs that use droop based controllers, which does not require the use of fast links of communications between the sources. The *SoC*-Sharing Function relies on two main features: the transient compensation and ESS equalization. The transient compensation is useful mostly to applications with slow dynamic response sources, such as FCs. The equalization feature is implemented with the aim to equalize the available energy that the batteries connected to the MG can absorb or discharge.

The effectiveness of the proposed algorithm was evaluated using a dc MG with two Li-Ion batteries and one FC. In this context, the MG stability was performed by linearizing the full MG model using the Lyapunov's Indirect Method. Finally, the experimental results, the computational simulation using PSIM and the numerical results solving in Matlab of the MG model were compared under different conditions of load and *SoC* to prove the effectiveness of the stability analysis and the proposed algorithm operation.

REFERENCES

[1] G. Wang, G. Konstantinou, C. D. Townsend, J. Pou, S. Vazquez, G. D. Demetriades, and V. G. Agelidis, "A review of power electronics for grid connection of utility-scale battery energy storage systems," *IEEE Trans. Sustain. Energy*, vol. 7, no. 4, pp. 1778–1790, Oct. 2016.

[2] K. Benmouiza and A. Cheknane, "Analysis of proton exchange membrane fuel cells voltage drops for different operating parameters," *Int. J. Hydrogen Energy*, vol. 43, no. 6, pp. 3512–3519, Feb. 2018.

[3] N. L. Diaz, T. Dragicevic, J. C. Vasquez, and J. M. Guerrero, "Intelligent distributed generation and storage units for DC Microgrids—A new concept on cooperative control without communications beyond droop control," *IEEE Trans. Smart Grid*, vol. 5, no. 5, pp. 2476–2485, Sep. 2014.

[4] N. L. Diaz, J. C. Vasquez, and J. M. Guerrero, "A communication-less distributed control architecture for islanded microgrids with renewable generation and storage," *IEEE Trans. Power Electron.*, vol. 33, no. 3, pp. 1922–1939, Mar. 2018.

[5] N. L. Diaz, A. C. Luna, J. C. Vasquez, and J. M. Guerrero, "Centralized control architecture for coordination of distributed renewable generation and energy storage in islanded AC microgrids," *IEEE Trans. Power Electron.*, vol. 32, no. 7, pp. 5202–5213, Jul. 2017.

[6] V. Nayanar, N. Kumaresan, and N. Ammasai Gounden, "A Single-Sensor-Based MPPT controller for wind-driven induction generators supplying DC microgrid," *IEEE Trans. Power Electron.*, vol. 31, no. 2, pp. 1161–1172, Feb. 2016.

[7] H.-J. Choi and J.-H. Jung, "Enhanced power line communication strategy for DC microgrids using switching frequency modulation of power converters," *IEEE Trans. Power Electron.*, vol. 32, no. 6, pp. 4140–4144, Jun. 2017.

[8] J. Yu, C. Dou, and X. Li, "MAS-based energy management strategies for a hybrid energy generation system," *IEEE Trans. Ind. Electron.*, vol. 63, no. 6, pp. 3756–3764, Jun. 2016.
[9] H. Qian, J. Zhang, J.-S. Lai, and W. Yu, "A high-efficiency grid-tie battery energy storage system," *IEEE Trans. Power Electron.*, vol. 26, no. 3, pp. 886–896, Mar. 2011.
[10] T. R. Oliveira, W. W. A. Goncalves Silva, and P. F. Donoso-Garcia, "Distributed secondary level control for energy storage management in DC microgrids," *IEEE Trans. Smart Grid*, vol. 8, no. 6, pp. 2597–2607, Nov. 2017.
[11] Q. Shafiee, T. Dragicevic, J. C. Vasquez, and J. M. Guerrero, "Hierarchical control for multiple DC-microgrids clusters," *IEEE Trans. Energy Convers.*, vol. 29, no. 4, pp. 922–933, Dec. 2014.
[12] M. Jarnut, S. Wermiński, and B. Waśkowicz, "Comparative analysis of selected energy storage technologies for prosumer-owned microgrids," *Renew. Sustain. Energy Rev.*, vol. 74, pp. 925–937, Jul. 2017.
[13] C. R. de Aguiar, G. H. F. Fuzato, R. Q. Machado, and J. M. Guerrero, "An adaptive power sharing control for management of DC microgrids powered by fuel cell and storage system," *IEEE Trans. Ind. Electron.*, vol. 67, no. 5, pp. 3726–3735, May 2020.
[14] T. Zhou and W. Sun, "Improved droop control based on virtual reactance for battery cycle life equalisation management in microgrid," *IET Gener., Transmiss. Distrib.*, vol. 12, no. 14, pp. 3435–3441, Aug. 2018.
[15] W. Han, C. Zou, C. Zhou, and L. Zhang, "Estimation of cell SOC evolution and system performance in module-based battery charge equalization systems," *IEEE Trans. Smart Grid*, vol. 10, no. 5, pp. 4717–4728, Sep. 2019.
[16] X. Lu, K. Sun, J. M. Guerrero, J. C. Vasquez, and L. Huang, "Double-quadrant State-of-Charge-Based droop control method for distributed energy storage systems in autonomous DC microgrids," *IEEE Trans. Smart Grid*, vol. 6, no. 1, pp. 147–157, Jan. 2015.
[17] N. Tashakor, E. Farjah, and T. Ghanbari, "A bidirectional battery charger with modular integrated charge equalization circuit," *IEEE Trans. Power Electron.*, vol. 32, no. 3, pp. 2133–2145, Mar. 2017.
[18] T. Dragicevic, J. M. Guerrero, J. C. Vasquez, and D. Skrlec, "Supervisory control of an adaptive-droop regulated DC microgrid with battery management capability," *IEEE Trans. Power Electron.*, vol. 29, no. 2, pp. 695–706, Feb. 2014.
[19] Y. Xia, M. Yu, P. Yang, Y. Peng, and W. Wei, "Generation-storage coordination for islanded DC microgrids dominated by PV generators," *IEEE Trans. Energy Convers.*, vol. 34, no. 1, pp. 130–138, Mar. 2019.
[20] G. H. F. Fuzato, K. D. A. Ottoboni, R. F. Bastos, C. R. Aguiar, and R. Q. Machado, "Voltage gain analysis of the interleaved boost with voltage multiplier converter used as electronic interface for fuel cells systems," *IET Power Electron.*, vol. 9, no. 9, pp. 1842–1851, Jul. 2016.
[21] K. Jin, M. Yang, X. Ruan, and M. Xu, "Three-level bidirectional converter for fuel-Cell/Battery hybrid power system," *IEEE Trans. Ind. Electron.*, vol. 57, no. 6, pp. 1976–1986, Jun. 2010.
[22] Z. Shuai, D. He, J. Wang, Z. J. Shen, J. Fang, and C. Tu, "Robust droop control of DC distribution networks," *IET Renew. Power Gener.*, vol. 10, no. 6, pp. 807–814, Jul. 2016.
[23] L. Meng, T. Dragicevic, J. C. Vasquez, and J. M. Guerrero, "Tertiary and secondary control levels for efficiency optimization and system damping in droop controlled DC–DC converters," *IEEE Trans. Smart Grid*, vol. 6, no. 6, pp. 2615–2626, Nov. 2015.
[24] C. Wang and M. H. Nehrir, "Load transient mitigation for stand-alone fuel cell power generation systems," *IEEE Trans. Energy Convers.*, vol. 22, no. 4, pp. 864–872, Dec. 2007.
[25] D. Zheng, H. Wang, J. An, J. Chen, H. Pan, and L. Chen, "Real-time estimation of battery state of charge with metabolic grey model and LabVIEW platform," *IEEE Access*, vol. 6, pp. 13170–13180, 2018.
[26] Y. Wang, P. Zhang, W. Li, W. Xiao, and A. Abdollahi, "Online overvoltage prevention control of photovoltaic generators in microgrids," *IEEE Trans. Smart Grid*, vol. 3, no. 4, pp. 2071–2078, Dec. 2012.
[27] G. H. F. Fuzato, C. R. Aguiar, R. F. Bastos, and R. Q. Machado, "Evaluation of an interleaved boost converter powered by fuel cells and connected to the grid via voltage source inverter," *IET Power Electron.*, vol. 11, no. 10, pp. 1661–1672, Aug. 2018.
[28] A. J. del Real, A. Arce, and C. Bordons, "Development and experimental validation of a PEM fuel cell dynamic model," *J. Power Sources*, vol. 173, no. 1, pp. 310–324, Nov. 2007.

THALES AUGUSTO FAGUNDES was born in Jundiaí, Brazil, in 1992. He received the B.S. degree in electrical engineering and the M.S. degree from the University of São Paulo, in 2017 and 2020, respectively, where he is currently pursuing the Ph.D. degree in electrical engineering. His main research interests are in the field of microgrids, energy management, and dc–dc converters for renewable energy sources and storage systems.

GUILHERME HENRIQUE FAVARO FUZATO was born in Varginha, Brazil, in 1989. He received the B.S. degree in electrical engineering, the M.S. degree in power electronics and dynamic systems, and the Ph.D. degree in microgrids from the University of São Paulo, in 2011, 2015, and 2019, respectively. From 2018 to 2019, he was a Visiting Researcher with the University of Aalborg. From 2012 to 2013, he worked at Siemens as a Field Service Engineer in automation area. From 2014 to 2015, he worked at Bosch with power electronics in automotive applications as a Temporary Researcher. Since 2016, he has been working as a Lecturer with the Federal Institute of Education, Science and Technology of São Paulo. His main research interests are in the fields of microgrids, energy management, and dc–dc converter for renewable energy sources and storage systems.

CASSIUS ROSSI DE AGUIAR was born in Santa Maria, Brazil. He received the bachelor's degree in electrical engineering from the Federal University of Santa Maria, Santa Maria, in 2008, and the master's and Ph.D. degrees in electrical engineering from the University of São Paulo, São Paulo, Brazil, in 2013 and 2016, respectively. He is currently a Professor with the Federal University of Technology–Paraná, Toledo, Brazil. His main research interests include microgrids, energy management, and dc–dc converters for renewable and storage systems.

KLEBBER DE ARAUJO OTTOBONI was born in Goiânia, Brazil, in 1992. He received the B.E. degree in electrical engineering from the Federal University of Goias, Goiania, Brazil, in 2013, and the M.Sc. and Ph.D. degrees in electrical engineering from the University of São Paulo, in 2016 and 2020, respectively. His main research interests are fractional order control, distributed generation systems, control of renewable energy sources, and heuristic optimization.

MAURICIO BICZKOWSKI received the B.S. degree in electrical engineering and the degree of specialist in energy efficiency from the Federal University of Technology Paraná, Brazil, in 2007 and 2013, respectively. From 2010 to 2016, he was an Assistant Professor with the School of Campos Gerais in Ponta Grossa and an Engineer with the Paraná Refinery, Brazil. He is currently an Engineer of maintenance, automation, protection and control at the superintendence of smart grids and special projects—Copel Distribution. His main research interests are: digital switching, voice and data transmission, oracle database, and among others.

RICARDO QUADROS MACHADO (Senior Member, IEEE) was born in Santa Maria, Brazil. He received the B.S. degree from the University of Santa Maria, Santa Maria, Brazil, in 1997, and the M.S. and Ph.D. degrees in electrical engineering from the University of Campinas, Campinas, Brazil, in 2000 and 2005, respectively. From 2002 to 2003, he was a Visiting Researcher with the University of Padova, Padova, Italy. From 2005 to 2007, he was a Postdoctoral Researcher with the Federal University of Santa Maria, Santa Maria. From 2013 to 2014, he was a Visiting Professor with the University of Toronto, Toronto, Canada. Additionally, from 2007 to 2018, he was an Assistant Professor with the University of São Paulo, São Carlos, Brazil. He is currently an Associate Professor with the University of São Paulo. His main research interests are: processing of energy in dc/dc and dc/ac converters, digital control of power converters, distributed generation systems, and smart grids and control of renewable energy sources.